9. L. Fotiadis and R. Kaplan, *Thin Solid Films* **184**, 415 (1990).
10. P. M. Mooney, F. K. LeGoues, J. Tersoff, J. O. Chu, *J. Appl. Phys.* **75**, 3968 (1994).
11. E. D. Williams and N. C. Bartelt, *Science* **251**, 393 (1991).
12. B. S. Swartzentruber, N. Kitamura, M. G. Lagally, M. B. Webb, *Phys. Rev. B* **47**, 13432 (1993).
13. J. Wei, X.-S. Wang, J. L. Goldberg, N. C. Bartelt, E. D. Williams, *Phys. Rev. Lett.* **68**, 3885 (1992).
14. B. Li, thesis, University of Maryland (1993).
15. A. A. Baski and L. J. Whitman, *Phys. Rev. Lett.* **74**, 956 (1995).
16. Independent evidence for the stability of Si(5 5 12) has recently been found in x-ray scattering measurements: S. Song, M. Yoon, S. G. J. Mochrie, *Surf. Sci.* **334**, 153 (1995).
17. P. J. Bedrossian, *Phys. Rev. Lett.* **74**, 3648 (1995).
18. R. M. Feenstra and J. A. Stroscio, *ibid.* **59**, 2173 (1987).
19. A modest buckling of 0.10 Å was assumed for the π-bonded chain atoms in the primary rows. This buckling is considerably smaller than the 0.45 Å buckling predicted for the Si(111)2 × 1 Pandey π-bonded chain, whose seven-member rings allow for greater structural flexibility. See, for example, J. E. Northrup, M. S. Hybertsen, S. G. Louie, *Phys. Rev. Lett.* **66**, 500 (1991).
20. This calculation assumes that the π-bonded chains reduce the effective number of dangling bonds on the chain by a factor of 2.
21. S. C. Erwin, M. R. Pederson, W. E. Pickett, *Phys. Rev. B* **41**, 10437 (1990).
22. Given the large size of the (5 5 12) unit cell, the following two simplifications were introduced to make the LDA calculation tractable: (i) The simulated images for the (5 5 12) surface were approximated by treating each of the three subunits [(225), (337) with a secondary row, and (337) with a tertiary row] as separate periodic surfaces, then combining the resulting images to form a single composite image. (ii) Structural relaxation was not performed on the entire structure; instead, atomic positions were fixed according to the theoretical local geometries of the proposed structural units.
23. As a result of a number of computational approximations, we expect topographical features in the simulated images to show better resolution and less diffuse character than corresponding features observed in STM images, particularly for the empty states. (i) The approximation of the tunneling matrix element by a constant neglects any role of the tip structure in degrading image resolution. (ii) The low average height $z \approx 3$ Å in the simulations, approximately half the experimental tip-surface distance, results in more localized features. Note that this height is determined by the chosen integrated local-state density $n = 10^{-6}$ electrons/bohr^3, which is constrained by the relatively narrow vacuum region separating adjacent slabs in the calculation. (iii) The relatively small basis set limits the extended nature of the unoccupied conduction states. (iv) The approximation of Brillouin-zone sums by a single point at the zone center (k = 0) artificially emphasizes the localization of unoccupied π-bonded surface states, which have antibonding character at the zone center.
24. The symmetry inequivalence of the two atoms on either side of the chain opens a gap in the corresponding surface state, with the occupied bonding combinations favoring the upper chain atom (that is, filled-state maxima are more pronounced to the left) and the antibonding combination favoring the lower chain atom (that is, empty-state maxima are more pronounced to the right).
25. D. J. Chadi, *Phys. Rev. B* **29**, 785 (1984).
26. I. Štich, M. C. Payne, R. D. King-Smith, J.-S. Lin, *Phys. Rev. Lett.* **68**, 1351 (1992).
27. K. D. Brommer, M. Needels, B. E. Larson, J. D. Joannopoulos, *ibid.*, p. 1355.
28. A clean Si(337) surface is composed of (5 5 12) terraces separated by step bunches or short (111)7 × 7 facets.
29. S. C. Erwin, A. A. Baski, L. J. Whitman, unpublished.
30. We are grateful to S. G. J. Mochrie for providing us with results prior to publication. This work was funded by the Office of Naval Research and a Naval Research Laboratory/National Research Council Postdoctoral Fellowship (A.A.B.), and was supported in part by a grant of high-performance computing time from the Department of Defense Shared Resource Center MAUI.

22 May 1995; accepted 3 July 1995

Organic Heterostructure Field-Effect Transistors

A. Dodabalapur,* H. E. Katz, L. Torsi,† R. C. Haddon

Organic field-effect transistors have been developed that function as either n-channel or p-channel devices, depending on the gate bias. The two active materials are α-hexathienylene (α-6T) and C_{60}. The characteristics of these devices depend mainly on the molecular orbital energy levels and transport properties of α-6T and C_{60}. The observed effects are not unique to the two materials chosen and can be quite universal provided certain conditions are met. The device can be used as a building block to form low-cost, low-power complementary integrated circuits.

Organic transistors have characteristics that make them attractive in applications such as large-area electronics, including low-cost deposition processes, compatibility with plastic substrates, and steadily improving performance. Thin-film transistors (TFTs) with active materials consisting of oligomers of thiophene have been pioneered by Garnier *et al.* (*1*); they are p-channel transistors and work in the accumulation and depletion modes but never in the inversion mode. We have recently shown that field-effect mobilities of $\mu = 0.01$ to 0.05 cm^2 V^{-1} s^{-1} and on-off current ratios greater than 10^6 are achievable with such materials (*2*, *3*). The field-induced conductance is independent of the thickness of the organic active material. The switching speeds of α-6T TFTs, which depend on bias conditions and device dimensions, are typically ~10 μs; hence, such TFTs are fast enough to be considered for use in display applications.

A few organic materials such as C_{60} have been used to make n-channel TFTs (*4*). These devices operate in the accumulation mode and, like the oligothiophenes, can never operate in the inversion mode. Recent work by Haddon *et al.* has resulted in C_{60} TFTs with $\mu = 0.08$ cm^2 V^{-1} s^{-1} in vacuum (*5*). Because neither oligothiophene nor fullerene transistors operate under inversion mode conditions, it is not possible to realize n- and p-channel operation from a single material. We have developed an organic transistor structure with two active materials that permits both p-channel and n-channel operation in a single device. The availability of such a device should enable the fabrication of complementary circuits that possess well-known advantages with respect to power dissipation and device lifetime. The operating characteristics of the device also show that heterojunction concepts can be applied to organic semiconductors.

AT&T Bell Laboratories, 600 Mountain Avenue, Murray Hill, NJ 07974, USA.

*To whom correspondence should be addressed.
†On leave from the Department of Chemistry, University of Bari, Bari I70126, Italy.

The schematic layer structure of the device is shown in Fig. 1. The first active layer (adjacent to the gate dielectric) is α-6T, a thiophene oligomer that exhibits good p-channel operation (*1*, *2*); this layer is typically 10 to 20 nm thick. The second layer, for n-channel operation, is C_{60} and is about 20 to 40 nm thick. A third electrically inactive organic layer is deposited on top of C_{60} to protect it from the ambient. The two active materials were chosen not only because good p-channel and n-channel transistors have been made with them, but also because the energy levels of their highest occupied and lowest unoccupied molecular orbitals (HOMOs and LUMOs) are favorable (Fig. 2). The energy levels of α-6T were taken from (*6*), in which they were measured by photoemission spectroscopy. The energy levels of –3.8 eV (LUMO) and –7.1 eV (HOMO) for C_{60} thin films were taken from (*7*). These values, which are usually measured under high vacuum conditions, may be slightly altered in devices that undergo some exposure to air. The energy levels of the HOMOs and LUMOs of the two materials are such that when the gate is biased negatively with respect to the source, the p-channel material (α-6T) is filled with holes, and when the gate is biased positively, the n-channel material (C_{60}) is filled with electrons. The energy band diagrams for the two modes of operation are shown in Fig. 3, where it is tacitly assumed that the magnitudes of the energy level discontinuities at the heterojunction remain unchanged under all bias conditions.

With two active materials, the same transistor can be used as either an n-channel or a p-channel device (Fig. 4). The

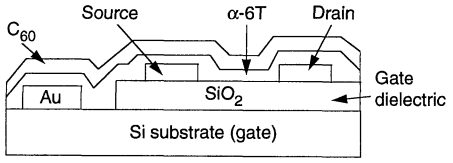

Fig. 1. Schematic layer structure of a heterojunction organic TFT with α-6T and C_{60} active layers. The dimensions are not to scale.

devices were tested by direct probing with coaxial probes under vacuum after exposing them to air for a few minutes between deposition and characterization. The device characteristics described above convincingly demonstrate the applicability of heterojunction concepts and design techniques to organic-polymeric materials. To show that the effects described above are not restricted to the particular materials chosen (α-6T and C_{60}), we changed the p-channel material to α,ω-dihexyl hexathienylene (8), another promising oligothiophene derivative. Characteristics qualitatively similar to those shown in Fig. 4 were obtained in these transistors; this finding implies that the observed behavior is not unique to the α-6T–C_{60} combination. Similar behavior has been observed with the α-6T–perylenetetracarboxylic anhydride material system and may be expected, in principle (9), for other combinations of organic-polymeric materials that have a band lineup similar to that in Fig. 2 as well as the appropriate transport properties.

The transistor characteristics shown in Fig. 4 were analyzed with a model developed for organic TFTs (*10*) that takes into account short-channel effects, parasitic resistance, and field dependence of the mobility. The p-channel operational characteristics of the device are almost identical to those of TFTs with only α-6T active layers (μ = ~0.004 cm^2 V^{-1} s^{-1}; threshold voltage = ~0 V). The n-channel characteristics are slightly different from those of TFTs with only C_{60} active layers. The threshold voltage is larger (+40 V); for small gate voltages there is a leakage component to the drain-

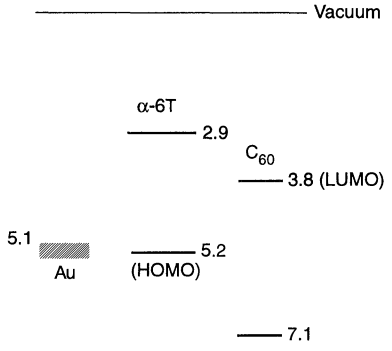

Fig. 2. Energy levels (in electron volts) of the HOMO and LUMO of α-6T [from (*6*)] and C_{60} [from (*7*)].

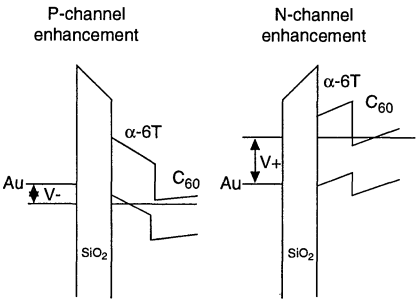

Fig. 3. Energy band diagrams of the heterojunction transistor in the p-channel and n-channel modes of operation. In the p-channel mode, an accumulation layer of holes is formed at the α-6T–SiO_2 interface; in the n-channel mode, an accumulation layer of electrons is formed in C_{60} near the interface with α-6T.

source current (shown in Fig. 4B by dotted lines), which disappears as the gate voltage increases beyond the threshold voltage. Beyond this point, the transistor characteristics are quite similar to those of C_{60} TFTs (*5*). The magnitude of the drain-source current at different gate biases is shown in Fig. 5. The n-channel field-effect mobility is calculated to be μ = 0.005 cm^2 V^{-1} s^{-1}.

The drain-source offset voltage present during n-channel operation is probably related to the choice of source and drain ohmic contacts. The work function of Au (5.1 to 5.2 eV) is almost exactly matched to the HOMO energy of the α-6T but poorly matched to the LUMO energy of the C_{60}. A potential barrier of >1 V exists between the

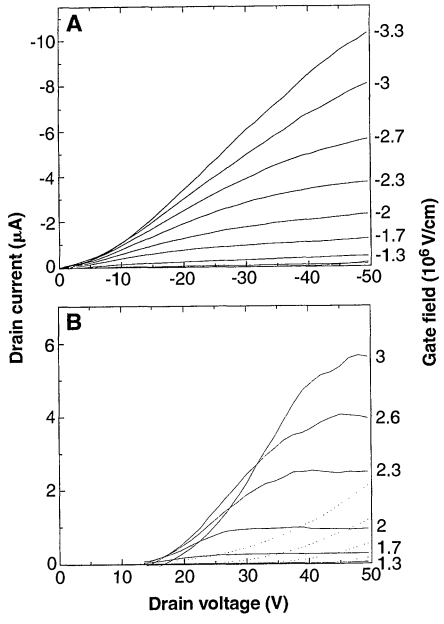

Fig. 4. Current-voltage characteristics are shown for p-channel operation (**A**) and n-channel operation (**B**) of a device with gate a length of 4 μm. The vertical gate electric field is also shown for both cases. The dotted lines in (B) represent the leakage component of the drain current.

work function of Au and the LUMO energy of the C_{60}. Another possible contributing factor to the offset is that electrons must pass through 10 to 20 nm of α-6T between the injecting contacts and the C_{60}. Further optimization of the contact metallization and device geometry should reduce both the threshold voltage and the drain-source offset voltage.

If the α-6T layer (Fig. 1) was too thick (>40 nm) it was not possible to obtain n-channel operation, whereas when the thickness was <25 nm, n-channel behavior always resulted. This behavior may occur because, as a result of electric field–induced band-bending, the LUMO energy of the α-6T at the interface with the gate dielectric becomes lower than the LUMO energy of the C_{60} near the interface with the α-6T. Because some of the electrons in the C_{60} may occupy very low mobility states (the most probable cause for the positive threshold voltage), there is a maximum thickness limit for the α-6T beyond which the field-induced electrons will occupy states in α-6T instead of in C_{60}.

The order of the two materials was reversed in some samples, with C_{60} deposited first. In such devices, good n-channel behavior (μ = 0.09 cm^2 V^{-1} s^{-1}) was observed. However, for negative gate biases, p-channel behavior was observable but the field-effect mobility was lower by several orders of magnitude. The hole mobility in α-6T depends critically on the quality of the films, the orientation of the α-6T molecules, and the nature of the surface on which the films are deposited. It is likely that the predeposited C_{60} causes a substantial degradation in the transport properties of the α-6T by inducing a different orientation than that induced by the SiO_2.

The above data shed some light on why many organic materials conduct only one carrier species (electrons or holes) efficiently at room temperature. The most reason-

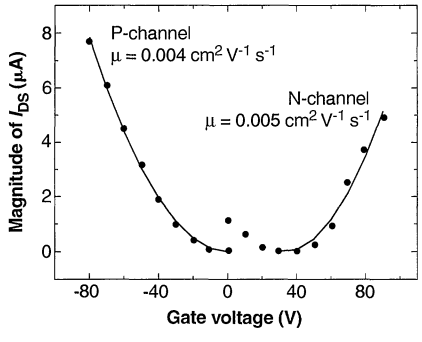

Fig. 5. Magnitude of the drain-source current I_{DS} as a function of gate voltage for the n- and p-channel modes of operation ($|V_{DS}|$ = 40 V). The solid lines are the data and the points are a parabolic fit from which the field-effect mobilities were extracted.

able explanation for this phenomenon is that the other species (electrons in α-6T and holes in C_{60}) become trapped in extremely low mobility states. The data in Fig. 4 and the energy level lineup in Fig. 2 suggest that the energies of such trap levels are not too far from the appropriate HOMO-LUMO energy levels. Were this not the case, and if the traps were very deep, the complementary behavior seen in these transistors would not be possible. For example, field-induced electrons, instead of occupying high-mobility states in C_{60} (Fig. 3B), might become trapped in lower lying low-mobility trap states in α-6T. The densities of the interface states (at the SiO_2–α-6T and α-6T–C_{60} interfaces) are also low enough not to seriously affect the bending of energy levels (Fig. 3) with bias.

Our observations suggest that heterojunctions based on organic materials have important similarities with their inorganic counterparts, including an approximate conformity with the so-called electron affinity rule, which prescribes the manner in which energy levels line up when a heterojunction is formed (*11*). More important, the transistor behavior indicates that the magnitude of the HOMO-LUMO discontinuities remains substantially unchanged under bias conditions. One of the practical applications of this work is the use of organic transistors in the fabrication of low-power digital circuits. Complementary circuits (which require n-channel and p-channel transistors) dissipate very little power because most of the transistors pass current only for brief periods when they are being switched (*12*); thus, in this application they can offer the dual advantages of lower power dissipation and extended device lifetime. The latter advantage is considered especially beneficial for organic-polymeric transistors.

REFERENCES

1. F. Garnier *et al.*, *Adv. Mater.* **2**, 592 (1990).
2. H. E. Katz, A. Dodabalapur, L. Torsi, A. J. Lovinger, R. Ruel, *Proc. Am. Chem. Soc. Div. Polym. Mater. Sci. Eng.* **72**, 467 (1995).
3. A. Dodabalapur, L. Torsi, H. E. Katz, *Science* **268**, 270 (1995).
4. J. Kastner, J. Paloheimo, H. Kuzmany, in *Springer Series in Solid State Sciences*, H. Kuzmany, M. Mehring, J. Fjink, Eds. (Springer-Verlag, Berlin, 1993), vol. 113, pp. 512–515.
5. R. C. Haddon *et al.*, *Appl. Phys. Lett.* **67**, 121 (1995).
6. C. Hosokawa *et al.*, *ibid.* **62**, 3228 (1993).
7. T. R. Ohno *et al.*, *Phys. Rev. B* **44**, 13747 (1991); G. K. Wertheim and D. N. E. Buchanan, *ibid.* **50**, 11070 (1994); G. K. Wertheim, personal communication.
8. F. Garnier, R. Hajlaoui, A. Yassar, P. Srivastava, *Science* **265**, 1684 (1994).
9. A. Dodabalapur *et al.*, unpublished results.
10. L. Torsi, A. Dodabalapur, H. E. Katz, *J. Appl. Phys.* **78**, 1088 (1995).
11. F. Capasso and G. Margaritondo, Eds., *Heterojunction Band Discontinuities: Device Physics and Applications* (North-Holland, New York, 1987).
12. J. Millman, *Microelectronics: Digital and Analog Circuits and Systems* (McGraw-Hill, New York, 1979).

18 April 1995; accepted 14 July 1995

Observation and Origin of Self-Organized Textures in Agates

Peter J. Heaney* and Andrew M. Davis

One of the most impressive manifestations of spontaneous pattern generation in natural materials is iris agate, which contains submicrometer concentric striations that may cycle several thousand times within an individual specimen. Analysis by secondary ion mass spectroscopy and transmission electron microscopy identified the iris texture as alternating layers of fine-grained, highly defective chalcedony and coarse-grained low-defect quartz. This oscillatory zonation in defect concentration may be ascribed to Ostwald-Liesegang crystallization cycles from silica-rich fluids that are variably polymeric and monomeric. Periodic changes in defect concentration and grain size also are observed with wavelengths of hundreds of micrometers and of centimeters, so that agates reveal textural self-similarity over three length scales.

For centuries natural scientists have marveled at patterns within rocks and minerals that formed without the benefit of external templates, and researchers now are attempting to exploit these textures to infer the conditions that govern crystallization processes. Minerals that exhibit compositional zoning (for example, plagioclase, garnet, and augite) have been studied extensively to determine crystal growth rates and cyclic changes in their depositional environments (*1*). Chemists have investigated periodic and aperiodic oscillatory behavior in systems far from equilibrium to understand nonlinear reaction dynamics (*2*). Agates present one of the most spectacular examples of autonomous pattern generation in nature, and the textures exhibited by these concentrically banded bodies are common to a host of spherulitic materials (*3*). Here, we report an examination of iris banding in agates that reveals oscillations in defect concentration over three length scales; this finding suggests crystallization from fluids with fluctuating degrees of polymerization.

Agates form within gas cavities of volcanic host rocks when microcrystalline chalcedony fibers nucleate on vug walls and grow inward (*4*). Although the popularity of agate as a semiprecious gem derives from its colorful zonation, it is the nonpigmented iris banding that is most remarkable for its rhythmic uniformity. Iris bands appear as striations parallel to the cavity wall and perpendicular to the fiber axes, and thus they generate concentric rings. Cross-polarized light microscopy reveals that iris bands oscillate with respect to refractive index: Bands with indices similar to those of quartz alternate with bands having slightly lower refractive indices, and these oscillations may cycle 8000 times or more within a given sector of an agate (*5*, *6*). The wavelength of the oscillation varies from ~0.1 to 5 μm, and the modulation creates an optical diffraction grating for visible light, giving rise to the iridescence that is the hallmark of museum-quality iris agate (*7*, *8*). Though sometimes obscured by pigmentation, zones with iris banding are present in virtually all agates.

Explanations for the occurrence of oscillatory banding in agate have invoked rhythmic segregation of amorphous opal within chalcedony (*5*) and periodic changes in fiber orientation (*8*). Studies that used powder x-ray diffraction and transmission electron microscopy (TEM) do not support these interpretations (*9*–*11*). Frondel (*12*) has demonstrated by scanning electron microscopy (SEM) that the iris layers with lower refractive indices are more easily etched by hydrofluoric acid. He argued that disparate etching rates result from oscillations in hydroxyl content along the chalcedony fiber length; the more rapidly etched "H" bands are OH-rich and the more resistant "L" bands are OH-poor. Because even trace amounts of hydrogen dramatically weaken quartz crystals, the speciation of hydrogen in quartz has provoked numerous investigations (*13*).

To test the possibility that iris bands represent compositional oscillations along the fiber axes, we examined iris agates by secondary ion mass spectroscopy (SIMS). Iris agates were sectioned parallel to the bands, and elemental variation along the fibers normal to the banding was obtained by tunneling through the iris layers by means of $^{16}O^-$ ion bombardment (Fig. 1) (*14*). The coupled substitution $Al^{3+} + Na^+ \leftrightarrow Si^{4+}$ is well documented in chalcedony (*10*), and it is supported in our results by nearly identical count rates for Al and Na (Fig. 1A). This cation exchange suggests that concentration variations for Al and Na should fall exactly out of phase with those

P. J. Heaney, Department of Geological and Geophysical Sciences and Princeton Materials Institute, Princeton University, Princeton, NJ 08544, USA.
A. M. Davis, Enrico Fermi Institute, University of Chicago, 5640 South Ellis Avenue, Chicago, IL 60637, USA.
*To whom correspondence should be addressed.

References

[3] **Organic Transistors: Two-Dimensional Transport and Improved Electrical Characteristics**
A. Dodabalapur; L. Torsi; H. E. Katz
Science, New Series, Vol. 268, No. 5208. (Apr. 14, 1995), pp. 270-271.
Stable URL:
http://links.jstor.org/sici?sici=0036-8075%2819950414%293%3A268%3A5208%3C270%3AOTTTAI%3E2.0.CO%3B2-E

[8] **All-Polymer Field-Effect Transistor Realized by Printing Techniques**
Francis Garnier; Ryad Hajlaoui; Abderrahim Yassar; Pratima Srivastava
Science, New Series, Vol. 265, No. 5179. (Sep. 16, 1994), pp. 1684-1686.
Stable URL:
http://links.jstor.org/sici?sici=0036-8075%2819940916%293%3A265%3A5179%3C1684%3AAFTRBP%3E2.0.CO%3B2-C